CHARACTERIZATION OF ORBITS IN THE TRUNCATED AND FORCED NONLINEAR SHRÖDINGER MODEL

Eli Shlizerman
Faculty of Mathematics and Computer Science
The Weizmann Institute of Science, Israel
eli.shlizerman@weizmann.ac.il

Vered Rom-Kedar
Faculty of Mathematics and Computer Science
The Weizmann Institute of Science, Israel
vered.rom-kedar@weizmann.ac.il

Abstract

The truncated and forced non-linear Schrödinger (NLS) model is analyzed using a novel framework in which a hierarchy of bifurcations is constructed. Consequently, a classification of the types of instabilities which are expected to appear due to the forcing is provided; It is shown that by introducing the forcing frequency as a free parameter (it was set to one in most of the previous studies), the behavior near the plane wave solution for any periodic box length, in the relevant amplitude regime for the truncated system, may be set to one of six different types. Furthermore, three of the six types are associated with chaotic behavior and instabilities (homoclinic chaos, hyperbolic resonance and parabolic resonance). Finally, a simple statistical measure which distinguishes between the fundamentally different types of instabilities is proposed.

Key words

Hamiltonian chaos, Bifurcations, Parabolic resonance, forcing frequency.

1 Introduction

The one dimensional non-linear Schrödinger equation emerges as a first order model in a variety of fields in Physics - from high intensity laser beam propagation to Bose-Einstein condensation to water waves theory; since it is the lowest order normal form for the propagation of strongly nonlinear dispersive waves its appearance in such a wide range of applications is mathematically obvious (see [Haller, 1999] and references therein). The NLS is completely integrable in one dimension on the infinite line (or with periodic boundary conditions) and hence completely solvable. The realization that the integrable structure might not persist under small perturbations, lead, almost two decades ago [Bishop *et al.*, 1986][Bishop and Lomdahl, 1986], to the development of a program in which the influence of forcing and damping that break the integrability of the PDE is considered. This program included extensive numerical study of the perturbed PDE's which was presented in various forms. Since the phase space is infinite dimensional - it is indeed unclear which form supplies the best understanding of the solutions structure. It was then suggested that a finite dimensional model - a two mode Galerkin truncation of the perturbed NLS - faithfully describes the PDE dynamics when even and periodic boundary conditions are imposed and the L_2 norm of the initial data is not too large [Bishop *et al.*, 1990*b*; Bishop and Clifford, 1996; Bishop *et al.*, 1988; Cai *et al.*, 2002]. The study of the perturbed two-mode model and characterization of chaotic orbits in it is the main subject of this paper.

Previous investigation of the truncated system lead to the discovery of a new mechanism of instability - the hyperbolic resonance - by which homoclinic solutions to a lower dimensional resonance zone are created [Kovacic and Wiggins, 1992; G.Kovacic, 1993; Haller and Wiggins, 1995*b*; Haller and Wiggins, 1995*a*]. New methodologies and tools introduced to this PDE-ODE study have finally lead to a proof that the homoclinic resonance dynamics, and in particular the birth of new types of multi-pulse homoclinic orbits which is associated with it, has analogous behavior in the PDE setting (see [Haller, 1999; Cai *et al.*, 2002; McLaughlin and Shatah, 1998] and references therein).

Here we provide a global analysis of the ODE model, which includes a qualitative understanding of all the relevant instabilities in the reduced model and the developement of a statistical tool for distinguishing between these solutions numerically. The main tools we use for the analysis - the energy momentum bifurcation diagrams, Fomenko graphs and the hierarchy of bifurcations framework are developed in [Shlizerman and Rom-Kedar, 2005; Litvak-Hinenzon and Rom-Kedar, 2004], and rely upon the fundamental works of [Lerman and Umanskiy, 1998] and [Fomenko, 1991].

The paper is ordered as follows: In Sec. 2 we describe the NLS equation and the truncated two-mode model. In Sec. 3 we discuss the integrable structure and con-

struct the hierarchy of bifurcation for our model. In Sec. 4, we utilize the integrable structure analysis to define the six fundamentally different types of motion near the plane wave solution, and present various characteristics of the three types of chaotic solutions. We conclude in Sec. 5 by providing a statistical tool for classification of the neighboring chaotic orbits directly.

2 The NLS Equation

Consider the following forced and damped NLS equation:

$$-i\psi_T+\psi_{XX}+|\psi|^2\psi = i\varepsilon(\alpha\psi-\Lambda\psi_{XX}+\Gamma\exp(-i\Omega^2T)), \tag{1}$$

with periodic boundary conditions and with even solutions in X:

$$\psi(X,T)=\psi(X+L,T), \psi_X(0,T)=0.$$

Let

$$B=\psi\exp(i\Omega^2T). \tag{2}$$

Then B satisfies the same boundary conditions as ψ and the autonomous (time independent) equation:

$$-iB_T+B_{XX}+(|B|^2-\Omega^2)B = i\varepsilon(\alpha B-\Lambda B_{XX}+\Gamma). \tag{3}$$

This equation was extensively studied in the last two decades [Bishop *et al.*, 1990*a*; Bishop *et al.*, 1990*b*; Bishop and Clifford, 1996; Bishop *et al.*, 1988; Bishop *et al.*, 1986], and in this section we will mention only the relevant results. In this context, the perturbed NLS was first derived as a small amplitude envelope approximation of the damped driven Sine-Gordon Equation (SGE) when the driving force is in the near resonance frequency. Then, $\Omega=1$ and the only parameter appearing in the unperturbed system is the box size L.

The space of spatially uniform solutions ($B(X,T)=\frac{1}{\sqrt{2}}c(T)$) is invariant under the perturbed flow (1) and the unperturbed solutions are of the form $c(T)=|c(0)|\exp[i(\Omega^2-\frac{1}{2}|c(0)|^2)T+i\gamma(0)]$. Linear stability analysis of such solutions at $\varepsilon=0$ shows that there is exactly one unstable mode, $\cos\frac{2\pi}{L}X$, when

$$\frac{2\pi}{L}<|c(0)|\leq\frac{4\pi}{L} \tag{4}$$

whereas for lower values of $|c(0)|$ the plane wave solution is linearly stable (neutral). We see that for large box size the plane wave solution is unstable even for small amplitude, as expected.

Consider a two mode complex Fourier truncation for equation (3):

$$B_2(X,T)=\frac{1}{\sqrt{2}}c(T)+b(T)coskX, \tag{5}$$

where the periodic boundary conditions imply that

$$k=\frac{2\pi}{L}j,\ j\in Z_+, \tag{6}$$

and since we are interested in the first unstable mode we take $j=1$. Substituting this solution to the NLS equation (3), setting $\alpha=\Lambda=0$ and $\Gamma=1$, and neglecting (see [Bishop *et al.*, 1990*a*; Bishop *et al.*, 1990*b*; Bishop and Clifford, 1996; Bishop *et al.*, 1988; Bishop *et al.*, 1986; Bishop *et al.*, 1983; Bishop and Lomdahl, 1986; Cai *et al.*, 2002] for discussion of this step) higher Fourier modes, we obtain the following equations of motion:

$$\begin{aligned}
&-i\dot{c}+\left(\frac{1}{2}|c|^2+\frac{1}{2}|b|^2-\Omega^2\right)c+\frac{1}{2}(cb^*+bc^*)b=i\sqrt{2}\varepsilon \\
&-i\dot{b}+\left(\frac{1}{2}|c|^2+\frac{3}{4}|b|^2-(\Omega^2+k^2)\right)b+\frac{1}{2}(bc^*+cb^*)c=0.
\end{aligned} \tag{7}$$

Here $|b|$ is the amplitude of the first symmetric mode and $\frac{1}{\sqrt{2}}|c|$ is the amplitude of the plane wave. These equations are of the form of a two degrees of freedom near integrable Hamiltonian system with the Hamiltonian:

$$H(c,c^*,b,b^*;\varepsilon)=H_0(c,c^*,b,b^*)+\varepsilon H_1(c,c^*,b,b^*), \tag{8}$$

and the Poisson brackets $\{f,g\}=-2i\left(\langle\frac{\partial}{\partial c},\frac{\partial}{\partial c^*}\rangle+\langle\frac{\partial}{\partial b},\frac{\partial}{\partial b^*}\rangle\right)$, where

$$\begin{aligned}
H_0 &= \frac{1}{8}|c|^4+\frac{1}{2}|b|^2|c|^2+\frac{3}{16}|b|^4-\frac{1}{2}(\Omega^2+k^2)|b|^2 \\
&\quad -\frac{\Omega^2}{2}|c|^2+\frac{1}{8}(b^2c^{*2}+b^{*2}c^2) \\
H_1 &= \frac{-i}{\sqrt{2}}(c-c^*).
\end{aligned} \tag{9}$$

Furthermore, at $\varepsilon=0$, these equations possess an additional integral of motion:

$$I=\frac{1}{2}(|c|^2+|b|^2) \tag{10}$$

and thus are integrable, see [Bishop *et al.*, 1988; Bishop *et al.*, 1986; Cai *et al.*, 2002].

Remark 1. *We expect the two-mode model to apply for regions in which the plane wave solution has at most one unstable mode. Using 4 and 10 it follows that near the circle $b=0$ we should expect the analysis to be valid for $I\leq 2k^2$. Interestingly enough, we see that exactly at this I value the symmetric mode solutions lose their stability.*

To understand the perturbed motion of the truncated model we study the integrable structure by the general framework of "hierarchy of bifurcations". See [Shlizerman and Rom-Kedar, 2005; Shlizerman and Rom-Kedar, 2004; Litvak-Hinenzon and Rom-Kedar, 2004] for the description of this general framework.

3 Integrable Structure of the Truncated System

For the truncated system we consider the following transformation to generalized action angle co-ordinates for $c \neq 0$ [Kovacic and Wiggins, 1992]; taking

$$c = |c| \exp(i\gamma), \quad b = (x + iy) \exp(i\gamma) \tag{11}$$

so that $I = \frac{1}{2}(|c|^2 + x^2 + y^2)$, one obtains the generalized action angle canonical coordinates for the Hamiltonian:

$$H(x, y, I, \gamma) = H_0(x, y, I) + \varepsilon H_1(x, y, I, \gamma),$$

where

$$(I, \gamma) \in (R^+ \times T),$$
$$(x, y) \in B_I = \{(x, y) | 0 \leq x^2 + y^2 < 2I\}$$

and

$$\begin{aligned} H_0(x, y, I) &= \frac{1}{2}I^2 - \Omega^2 I + (I - \frac{1}{2}k^2)x^2 - \frac{7}{16}x^4 \\ &\quad - \frac{3}{8}x^2y^2 + \frac{1}{16}y^4 - \frac{1}{2}k^2y^2, \qquad (12) \\ H_1(x, y, I, \gamma) &= \sqrt{2}\sqrt{2I - x^2 - y^2}\sin\gamma. \qquad (13) \end{aligned}$$

The transformation to these variables is singular at $c = 0$, namely on the circle $2I = x^2 + y^2$, where the phase γ is ill defined and the perturbation term has a singular derivative. In Kovacic and Haller [Kovacic and Wiggins, 1992; G.Kovacic, 1993; Haller and Wiggins, 1995*b*; Haller and Wiggins, 1995*a*] the analysis was performed for phase space regions which are bounded away from this circle. Here, to better understand the dynamics near this circle, we introduce a similar transformation which is valid as long as $b \neq 0$:

$$b = |b|e^{i\theta}\ ,\ c = (u + iv)e^{i\theta}\ ,\ I = \frac{1}{2}(u^2 + v^2 + |b|^2) \tag{14}$$

We thus obtain the equation of motion in the canonical coordinates (u, v, I, θ) from the Hamiltonian:

$$\begin{aligned} H_0(u, v, I) &= \frac{3}{4}I^2 + \left(-\Omega^2 + \frac{3}{4}u^2 - \frac{1}{4}v^2 - k^2\right) I \\ &\quad - \frac{7}{16}u^4 - \frac{3}{8}u^2v^2 + \frac{1}{2}k^2u^2 + \frac{1}{2}k^2v^2 + \frac{1}{16}v^4 \\ H_1(u, v, I) &= \sqrt{2}(v\cos\theta + u\sin\theta). \end{aligned}$$

When both γ and θ are well defined, namely for $cb \neq 0$, the two sets of coordinates are simply related:

$$\begin{aligned} x &= |b|\cos(\theta - \gamma) & y &= |b|\sin(\theta - \gamma) \\ u &= \frac{|c|}{|b|}x, & v &= -\frac{|c|}{|b|}y. \end{aligned}$$

It follows that for $x^2 + y^2 < 2I$ we have:

$$\frac{d\gamma}{dt} = \omega(x, y, I) = I - \Omega^2 + x^2 = \frac{\partial H_0(x, y, I)}{\partial I} \tag{15}$$

and for $u^2 + v^2 < 2I$ we have:

$$\frac{d\theta}{dt} = \omega(u, v, I) = \frac{3}{2}I - \Omega^2 + \frac{3}{4}u^2 - \frac{1}{4}v^2 - k^2 = \frac{\partial H_0(u, v, I)}{\partial I}. \tag{16}$$

Consider the truncated model in appropriate generalized action angle co-ordinates, i.e. $H_0(q, p, I; k, \Omega)$ where (q, p) stands for either (x, y) or (u, v) in representation 11 and 14 respectively. Each energy surface is foliated by the level sets which are composed of either a few two dimensional tori, circles and possibly their separatrices or isolated fixed points. In our system there is only one isolated fixed point at $(q, p, I; k, \Omega) = (0, 0, 0; k, \Omega)$. A circle in the full phase space corresponds to an isolated fixed point in the normal plane (q, p), namely to a point $p_f = (q_f, p_f, I_f)$ at which $\frac{\partial H_0}{\partial q}\Big|_{p_f} = \frac{\partial H_0}{\partial p}\Big|_{p_f} = 0$. For our model, there are six families of such circles as listed in Table 1.

Following [Lerman and Umanskiy, 1998] terminology, the circles are called here singular circles and the curves of energy and action values $(H_0(p_f), I(p_f))$ corresponding to these circles are called singularity surfaces. The structure of these singularity surfaces, plotted in the energy-momentum space, serves as an organizing skeleton of the energy surfaces.

Locally, in the $(q, p, I; k, \Omega)$ coordinate system, the normal stability of an invariant circle is determined by $\det\left(\frac{\partial^2 H_0}{\partial^2(q,p)}\Big|_{p_f}\right) = -\lambda_{p_f}^2$. Indeed, when λ_{p_f} is real and non-vanishing the corresponding circle is said to be normally hyperbolic, when it vanishes it is called normally parabolic and when it is pure imaginary it is normally elliptic, see the detailed references in [Litvak-Hinenzon and Rom-Kedar, 2004] and the discussion in [Bolotin and Treschev, 2000]. For our example these calculations show that the first and third families of invariant circles become parabolic at $I = \frac{1}{2}k^2$ whereas the second and fourth families are parabolic at $I = 2k^2$.

3.1 Hierarchy of Bifurcations

We use two essential tools to describe the energy surfaces and the the singularity surfaces of the truncated model: the Energy Momentum Bifurcation Diagram (EMBD) and the Fomenko graphs (see section 3.2). We

Invariant circle: $\theta, \gamma \in T^1$	Exists For	Elliptic For	Hyperbolic For	Description
1. $p_{pw} = (x = 0, y = 0, I, \gamma)$	$I \geq 0$	$I < \frac{1}{2}k^2$	$I > \frac{1}{2}k^2$	Plane wave
2. $p_{sm} = (u = 0, v = 0, I, \theta)$	$I \geq 0$	$I < 2k^2$	$I > 2k^2$	Symmetric mode
3. $p^{\pm}_{pwm} =$				
$(x = \pm\sqrt{\frac{4}{7}(-k^2 + 2I)}, y = 0, I, \gamma)$	$I \geq \frac{1}{2}k^2$	$I \geq \frac{1}{2}k^2$	-	PW mixed mode
$(u = \pm\sqrt{\frac{6}{7}I + \frac{4}{7}k^2}, v = 0, I, \theta)$	$I > \frac{1}{2}k^2$	$I > \frac{1}{2}k^2$	-	”
4. $p^{\pm}_{smm} =$				
$(x = 0, y = \pm 2k, I, \gamma)$,	$I > 2k^2$	$I > 2k^2$	-	SM mixed mode
$(u = 0, v = \pm\sqrt{2I - 4k^2}, I, \theta)$	$I \geq 2k^2$	$I \geq 2k^2$	-	”

Table 1. Singular circles and their normal stability.

delineate the energy and parameter space of the integrable family of Hamiltonian systems $H_0(q, p, I; k, \Omega)$ by using these tools to construct the following hierarchy of bifurcations:

1. Single energy surface. The first level consists of the values of the constants of motion across which the topology of the level sets on a given energy surface $H_0(q, p, I; k, \Omega) = h$ is changed. These are the values at which the level sets include isolated circles, namely the values at which the singularity surfaces cross the vertical surface $H_0 = h$ on the EMBD, and thus these correspond to the vertices in the Fomenko graphs.
2. Energy bifurcation values. The second level consists of the energy bifurcation values h^b at which the form of the Fomenko graph changes, namely across which the energy surfaces are no longer equivalent. Thus, it describes how the energy surface differential topology is changed with h.
3. Parameter dependence of the energy bifurcation values. The third level consists of the bifurcating parameter values k^b, Ω^b at which the bifurcation sequence of the second level changes (by either changing the order of the energy bifurcating values or by adding/substracting one of the energy bifurcation values).

Next we will describe how we construct each level of the hierarchy for our model, and then we demonstrate numerically that typically each of these bifurcations is associated with a different type of perturbed motion in its vicinity.

$H_0(x_f, y_f, I)$ Evaluation
1. $H(x_{pw}, y_{pw}, I) = H(0, 0, I) = (\frac{I^2}{2} - \Omega^2 I)$
2. $H(u_{sm}, v_{sm}, I) = H(0, 0, I) = \frac{3}{4}I^2 - (k^2 + \Omega^2)I$
3. $H(x^{\pm}_{pwm}, y^{\pm}_{pwm}, I) = \frac{15}{14}I^2 - (\Omega^2 + \frac{4}{7}k^2)I + \frac{1}{7}k^4$
4. $H(u^{\pm}_{smm}, v^{\pm}_{smm}, I) = \frac{I^2}{2} - \Omega^2 I - k^4$

Table 2. Singular surfaces. Hamiltonian at the singular circles.

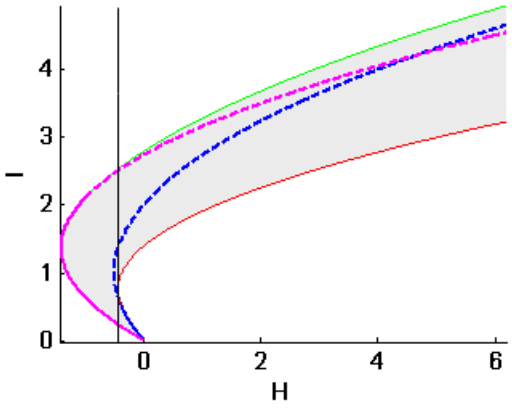

Figure 1. EMBD for $k = 1.025, \Omega = 1$.

3.2 Level 1: Single Energy Surfaces

Calculation of the singular surfaces and the normal stability of the lower dimensional tori are the first steps in depicting the global structure of the energy surfaces. The *energy-momentum bifurcation diagram (EMBD)* is constructed by plotting the singular surfaces -$(H_0(p_f(I)), I)$ in the (h, I) plane, where $(p_f(I))$ are given by the six families of Table 2.

In figure 1 we plot these curves for the non-dimensional wave number $k = 1.025$ and $\Omega^2 = 1$, the parameter values used in previous works [Bishop *et al.*, 1990*a*; Bishop *et al.*, 1990*b*; Bishop and Clifford, 1996; Bishop *et al.*, 1988; Bishop *et al.*, 1986; Bishop *et al.*, 1983]. We use the usual convention in bifurcation diagrams by which normally stable circles are denoted by solid lines whereas normally hyperbolic cir-

cles are denoted by dashed lines (see Table 1). Different colors are used for the different families of invariant circles (Thick and thin black line[1] for the plane wave and its bifurcating branch and thick and thin grey line[2] for the symmetric mode and its bifurcation branch). The allowed region of motion is shaded - for each point (h, I) in this shaded region there are (c, b) values satisfying $H_0(c, b) = h, I = \frac{1}{2}(|c|^2 + |b|^2)$. An energy surface in this diagram is represented by the intersection of a vertical line with the allowed region of motion. The topology of the level sets for different I values on a given energy surface is represented by the Fomenko graphs.

The Fomenko graphs are constructed by assigning to each connected component of the level sets (on the given energy surface) a point on the graph, so there is a one-to-one correspondence between them (see [Fomenko, 1991][Litvak-Hinenzon and Rom-Kedar, 2004]). Then, an edge of this graph corresponds to a regular one parameter family of two tori whereas vertices correspond to singular values of (h, I) at which some families of tori glue together or shrink to a singular circle. In the standard construction of the Fomenko graphs [Fomenko, 1991] the main objective is the study of the topology of the surfaces and the level sets, hence, for example, all the normally elliptic singular circles are assigned with the same symbol (molecule "A"). Here, we distinguish between the different singular circles as these correspond to different dynamic in the NLS. Thus, we denote the invariant circles corresponding to the plane wave family (p_{pw}) and the invariant circles which emanate from them ($p^{\pm}_{pwm}$), by open and full triangles respectively. The invariant circles corresponding to the symmetric mode family (p_{sm}) and the invariant circles which emanate from them ($p^{\pm}_{smm}$), are denoted by open and full circles. In this way the topological changes of the level sets are discovered and the energy surface may be reconstructed from these graphs.

The vertical line on Fig. 1 indicates the energy value for which the Fomenko graph is shown in Fig. 2. In this figure the relation between the energy momentum bifurcation diagram, the Fomenko graph and the energy surface is demonstrated. Projections of the energy surface are plotted twice; the energy surface is the two dimensional surface in the (x, y, I) space (respectively (u, v, I) space) multiplied, for all $c \neq 0$ (for all $b \neq 0$), by the circle $\gamma \in S^1$ ($\theta \in S^1$). The redundant presentation in the (u, v, I) space is shown to better explain the level sets topology near the circle $c = 0$ where the transformation to the (x, y, I) co-ordinates is singular.

We observe that these Fomenko graphs encode all needed information for the reconstruction of the energy surfaces, without the explicit computation of the corresponding energy surfaces[Fomenko, 1991]. In [Shlizerman and Rom-Kedar, 2005] we present the full sequence of Fomenko graphs for this model for several parameter values, and using the above coding the corresponding energy surfaces may be found. We note that a similar construction using branched surfaces for some n d.o.f. systems has been recently suggested (see [Litvak-Hinenzon and Rom-Kedar, 2004] and references therein).

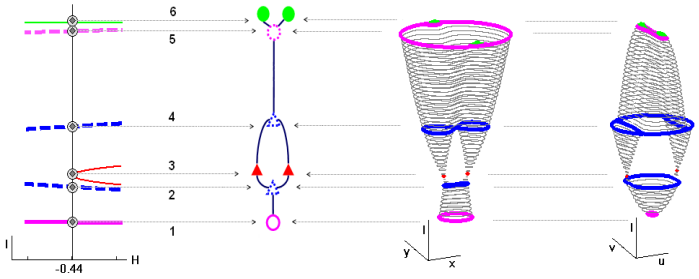

Figure 2. EMBD, Fomenko graph and energy surfaces (mode S^1) for $k = 1.025, \Omega = 1, h = -0.44$.

3.3 Level 2: Bifurcating Energy Values

Intersecting the energy-momentum bifurcation diagrams with a vertical line (hyper-surface in the n d.o.f. case) and constructing the corresponding Fomenko graphs (branched surfaces) leads to a full description of a given energy surface. It follows that many changes in the differential topology of the energy surfaces can be easily read off from these diagrams (the EMBD) - they correspond to singularities - folds, branchings, intersections or asymptotes - of the singularity surfaces. Furthermore, some of these singularities of the singularity surfaces are also associated with some dynamical phenomena (e.g. resonances and parabolicity). We will describe here only folds and branchings, as these are the only singularities of the plane wave curve which occur in the relevant range of I values, see [Shlizerman and Rom-Kedar, 2005] for the full analysis and description.

3.3.1 Folds in the singularity surfaces and Resonances Clearly (see for example Fig. 1) the energy surfaces change their topology whenever there is a fold in the singularity surfaces. Furthermore, it was established (see [Litvak-Hinenzon and Rom-Kedar, 2004]) that folds of non-parabolic singularity surfaces correspond to strong resonance relations for the lower dimensional invariant tori:

$$\frac{dH}{dI}(p_f^*) = 0 \Leftrightarrow \dot{\gamma}\Big|_{p_f^*} = 0.$$

In particular, a minima (or maxima) of the singularity surface $H_0(q_f, p_f, I_f)$ of the non-parabolic tori (q_f, p_f, I_f) corresponds to a circle of fixed points. Hence, to find a set of bifurcating energies we need to list the extremum of the surfaces $H_0(q_f, p_f, I_f)$ for

[1] blue and red
[2] magenta and green

the various singularity manifolds and verify that these are non-degenerate. In Table 3 we list the I values for which folds are created for the six singular surfaces of Table 2 and the values of I for which the singular circles are parabolic (Table 1).

I-resonance	I-parabolic	Parabolic Res.
1. $I_r^{pw} = \Omega^2$	$I_p^{pw} = \frac{1}{2}k^2$	$k_{pr-pw} = \sqrt{2}\Omega$
2. $I_r^{sm} = \frac{2k^2+2\Omega^2}{3}$	$I_p^{sm} = 2k^2$	$k_{pr-sm} = \sqrt{\frac{1}{2}}\Omega$
3. $I_r^{pwm} = \frac{4k^2+7\Omega^2}{15}$	$I_p^{pw} = \frac{1}{2}k^2$	$k_{pr-pw} = \sqrt{2}\Omega$
4. $I_r^{smm} = \Omega^2$	$I_p^{smm} = 2k^2$	$k_{pr-sm} = \sqrt{\frac{1}{2}}\Omega$

Table 3. Resonant and parabolic singular circles.

Using the resonant I values of Table 3 in Table 2 we conclude that the following energy values correspond to bifurcations due to the resonances/folds, of the plane wave branch:

$$h_r^{pw} = -\frac{1}{2}\Omega^4, \tag{17}$$

At this energy the corresponding family of circles p_{pw} has a circle of fixed points.

3.3.2 Branching surfaces and parabolic circles Another source for bifurcations in the energy surface structure appears when the singularity surface splits. For the two degree of freedom case such a splitting is associated with the appearance of a parabolic circle (for the n d.o.f. case we look for a fold in the surface of parabolic tori, namely we look for an $n-2$ resonant parabolic $n-1$ tori, see [Litvak-Hinenzon and Rom-Kedar, 2004] for precise statement). Thus, the appearance of the parabolic circle p_{sm} at $h = h_p^{sm}$ from which the branches of circles $p_{smm}^{\pm}$ emerge implies that for energies below this value no such circles appear, and the Fomenko graph has no splitting to two branches whereas larger energies have these two circles as the upper boundary of the energy surface. In Table 3 we list the parabolic values of I. Plugging these values in Table 2 we find an additional energy bifurcation value which is associated with the plane wave:

$$h_p^{pw} = \frac{1}{2}k^2(\frac{1}{4}k^2 - \Omega^2) \tag{18}$$

3.4 Level 3: Parametric Bifurcations

The EMBD clearly depends on the parameters of the problem, the wave number k and the forcing frequency Ω. When the order of the energy bifurcation values changes as these parameters are varied, a parametric bifurcation occurs. In Fig. 3 a bifurcation diagram of the energy bifurcation values associated with the plane wave is shown - the energy values at which the plane wave is resonant (h_{rpw}), parabolic (h_{ppw}) and the energy values at which the mixed mode solutions emanating from the plane wave solution are resonant (h_{rpwm}), are drawn as a function of Ω. *The crossing of these curves in the diagram corresponds to a bifurcation of the EMBDs*-for this value of Ω the plane wave is both resonant and parabolic, and the sequence of the Fomenko graphs changes across this value of Ω.

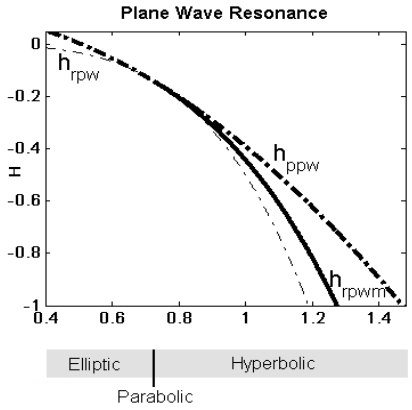

Figure 3. Bifurcation diagram of the energy bifurcation values for $k = 1.025$, Ω is varied.

Recall that our model is valid for relatively small periodic lengths, so that the NLS pde possesses only one linear unstable mode; therefore, L is traditionally chosen as $L \approx 6.12$ an thus $k \approx 1.025$. Another tradition in this context is to consider the NLS as a valid approximation of the SGE equation, which implies that $\Omega^2 \approx 1$. Studying the truncated perturbed NLS independently, we allow both parameters k and Ω to be free.

Repeating the construction of the integrable structure for the truncated system with these two free bifurcation parameters we find that the fixed points of the normal plane (x, y) and their stability depend only on k and this dependence does not change the order by which the solutions change their stability as I grows nor their type (see Table 1). However, constructing the next levels of the hierarchy reveals that the EMBD curves change with (k, Ω) (Table 2) and the bifurcating values (Table 3) change as well. Thus, *the parameter Ω provides additional control for the energy bifurcation values*. We show next that at these bifurcation values different types of chaotic behavior appear.

4 Temporal chaos near plane wave

We propose that the above detailed understanding of the unperturbed structure immediately translates into a qualitative understanding of the perturbed motion. Our main interest here is in the perturbed solutions near the spatially uniform plane wave.

The behavior near the the plane wave solution (singular surface 1 in table 2) depends primarily on its local stability and on the rotation rate on it ($\dot{\gamma}$). If it is a normally elliptic circle we have the usual Birkhoff normal

form/resonant behavior depending on the ratio between the normal and inner frequencies of the plane wave circle. When the plane wave corresponds to a hyperbolic circle, for sufficiently small perturbation its separatrices split and, if $\dot{\gamma}$ is bounded away from zero, the usual chaotic zone of area preserving maps appears in the Poincaré map in γ. We will refer to this behavior as *homoclinic chaos*. When the plane wave corresponds to a non-resonant parabolic circle, the perturbed motion near it stays close to the integrable circle just as in the elliptic case, since the separatrix is small and its splitting is exponentially small in the distance from the bifurcation point.

The behavior of the perturbed orbits changes dramatically near strong resonances; When the rotation rate vanishes ($\dot{\gamma} = 0$), the strongest resonance is created - a circle of fixed points appears. For normally elliptic resonant circles, perturbation leads to the usual resonance phenomena. When a normally hyperbolic circle becomes resonant, there is a family of heteroclinic orbits connecting pairs of fixed points on the circle. Under perturbation this family creates a *hyperbolic resonance* zone, see [Haller, 1999; Kovacic and Wiggins, 1992]. When the singular circle is parabolic and resonant - a *parabolic resonance* is created, and a small perturbation leads to dramatically different dynamics than in other types of resonances. The initial conditions near the invariant circle do not stay close to it as in the case of periodic motion on a non-resonant parabolic circle [Rom-Kedar, 1997]. We proceed by presenting the phase space and the numerical solutions of the perturbed orbits for the three fundamentally different types of chaotic motion described above: homoclinic chaos (which corresponds to a point on an unstable singular curve - a bifurcation of the first level), hyperbolic resonance (which corresponds to a fold - bifurcation of the second level) and parabolic resonance (which corresponds to a fold and branching at the same point - bifurcation of the third level).

Notice that once we have found the perturbed motion of the two-mode model we are able to recover $B(X,T)$ - the approximated solution of the NLS equation (5). The relation between the solution in the (x,y,I,γ) space to the truncated solution $B_2(X,T)$ and hence to the truncated solution $\psi_2(X,T) = B_2(X,T)\exp(-i\Omega^2 T)$ of the time dependent equation is easily found for $c \neq 0$ via the transformations (5,11):

$$\begin{aligned} B_2(X,T) &= (\sqrt{I(T) - \frac{1}{2}(x^2(T)+y^2(T))} \\ &\quad + (x(T)+iy(T))\cos kX)\exp(i\gamma(T)) \\ \psi_2(X,T) &= B_2(X,T)\exp(-i\Omega^2 T), \end{aligned} \tag{19}$$

To understand the nature of these solutions, we present them in several ways (Figs. 4, 5 and 6). In diagrams (A),(C),(F) and (G) of these figures we use the action angle coordinates (x,y,I,γ) to achieve an effective comparison between the perturbed and the underlying unperturbed structures. In addition to the standard (x,y) presentation of the Poincaré sections in γ we include the Probability Distribution Function (PDF) of the return times to the section.

In diagrams (B),(D) and (E) we do not apply any coordinate transformation and consider the recovered solution, which can be a solution of the NLS pde as well. In previous works it was suggested that plots of $|B(X,T)|$ as a function of (X,T) for a small interval of time (will be referred to as *the amplitude plot*) reveal the difference between regular and chaotic motion. Besides the space-time profiles (the amplitude plots) we construct similarly to [McLaughlin and Overman, 1995; Cai *et al.*, 2002], the diagram $(\mathrm{Re}\{B(0,T)\}, \mathrm{Im}\{B(0,T)\})$ for some interval T (we will call this representation a *B-plane plot*). We are allowed to consider the solution at $X = 0$, since in the autonomous NLS equation (2) the choice of even solutions ensures that the soliton will be centered at $X = 0$ or at $X = \pm\frac{L}{2}$.

In Sec. 3.4 we have shown that the parameters k and Ω^2 control the stability of the invariant circles and the rotation rate. By manipulating these parameters we are able to produce the three types of perturbed orbits which we discuss here. For consistency with the previous works [Bishop *et al.*, 1990*a*; Bishop *et al.*, 1990*b*] we have set the parameters in parabolic resonance and homoclinic chaos to $k = 1.025$ and have chosen to vary Ω. In the hyperbolic resonance case we have chosen to set (k,Ω) to $(0.8, \sqrt{1.79})$ for which the phase shift along the homoclinic loop is approximately π ($\Delta\gamma = \pi$). Then a stability island which shadows the resonance zone in the invariant plane is seen.

4.1 Homoclinic chaos and Hyperbolic resonance

Homoclinic chaos in the truncated model is formed when the plane wave possesses homoclinic loops, or in other words - unstable. From Table 1, we can predict that for $I^{pw} > \frac{1}{2}k^2$ the perturbed solutions near the plane wave will exhibit homoclinic chaos for almost all Ω values. The chaotic zone is created in the $x-y$ coordinates, with uniformity in the angle variable, since for almost all Ω the motion rate does not vanish ($|\dot{\gamma}| > 0$).

The motion near hyperbolic resonant circles is of completely different nature [Kovacic and Wiggins, 1992; G.Kovacic, 1993; Haller and Wiggins, 1995*b*; Haller and Wiggins, 1995*a*]. Of particular interest for the NLS model are the hyperbolic resonant plane wave circles which exist when $I_p^{pw} = \frac{1}{2}k^2 < I_r^{pw} = \Omega^2$. When $\Omega = 1$ these appear only for small wave numbers ($k < \sqrt{2}$), namely for sufficiently large intervals. By introducing the additional parameter Ω we see that *for any k value there is an interval of Ω values for which the resonant plane wave circle is hyperbolic*: it is hyperbolic for all $\Omega > \Omega_{pr-pw} = \frac{1}{\sqrt{2}}k$. Here, we show some perturbed trajectories which appear near the hyperbolic resonance regime. In Fig. 5 a trajectory which is trapped in a stability island is shown. We see that the main difference between the regular homoclinic chaos and the hyperbolic resonant chaotic motion

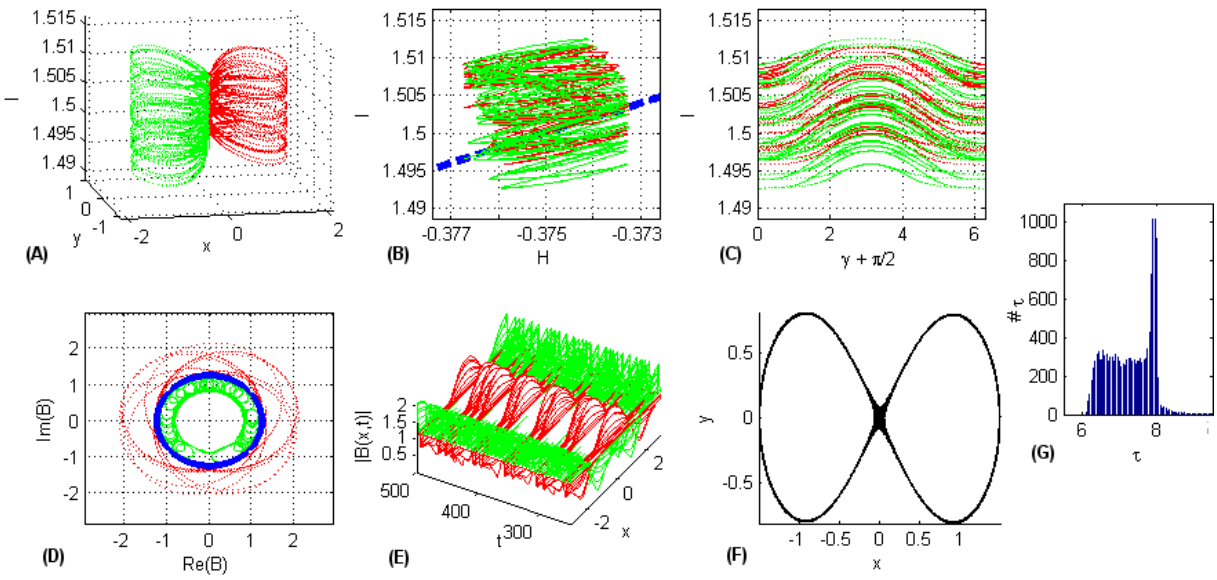

Figure 4. A perturbed orbit near a family of hyperbolic circles for $k = 1.025$, $\Omega^2 = 1$, $\varepsilon = \frac{1}{\sqrt{2}}10^{-4}$. Initial Conditions: $(c(0), b(0)) = (\sqrt{3}, 10^{-6})$ i.e. $(x(0), y(0), I(0), \gamma(0)) = (10^{-6}, 0, 1.5, 0)$. Red marker stands for a soliton centered at $X = 0$ (right side of the plane wave) and the green marker stands for a soliton centered at $X = \pm L/2$ (left side of the plane wave).

has to do with the non-uniformity in the angle variable - thus it is not observable in the amplitude plot but is clearly seen in the B plane plots. We also observe a spread of $O(\sqrt{\varepsilon})$ in (I, x, y) near the hyperbolic resonance regime, however the spread is not robust and depends strongly on the choice of initial conditions. In figure 4 we show the behavior near regular homoclinic orbits whereas figure 5 shows the behavior near resonant homoclinic orbits. We note that in these plots typical chaotic orbits are shown - these orbits shadow some of the countable infinity of multipulse homoclinic and heteroclinic orbits that exist due to the transverse separatrix crossings (see [Haller, 1999] and references therein).

4.2 Parabolic resonance

Parabolic resonance is a bifurcation in the energy surface structure, which appears when the singularity surface has a cusp and a fold of one of the branches (or split in the symmetric case). In Sec. 3.3.2 we found the energy function h_p^{pw} (Eq. 18) for bifurcations which appear due to singularity surface branchings. The behavior near a branching point is not simple - to analyze it one needs to understand how Hamiltonian trajectories cross bifurcations [Lebovitz and Pesci, 1995]. It appears that the action in the normal plane is a key ingredient in understanding the perturbed motion as it is adiabatically preserved [Neishtadt, 1975]. In Fig. 6 the difference between parabolic resonance and other types of motion is demonstrated numerically. This phenomenon can be described as a combination of a localization of elliptic resonance (can be seen in $(I-\gamma)$ plot) and instabilities due to hyperbolic resonance (can be seen in (x, y, I) plot). Notice the strong non-uniformity in the B-plane plot and the long tail which appears in the PDF of the return times. Finally, notice the paths of the trajectory in the EMBD plot which strongly suggests that indeed adiabatic description of some segments of the motion is appropriate.

It is important to notice that by remark 1, for all $\Omega < \sqrt{2}k$, the above scenarios of plane wave parabolic resonance, hyperbolic resonance and homoclinic chaos occur in the range at which the NLS has only one unstable mode.

5 Characterization of the perturbed solutions

Consider an even solution $B(X, t)$ of the perturbed NLS equation (Eq. 3) (either a solution of the PDE or a recovered truncated solution), and examine $|B(0, t)|$.

Our aim is to find the signatures of the different instabilities discussed above on the signal $|B(0, t)|$. Such a measure or a technique should suggest simple classification of the perturbed orbits and will be a good candidate for comparison of the truncated recovered solution with numerical solutions of the perturbed NLS equation. Though we can calculate the first two Fourier modes of such solutions and reconstruct the phase diagrams similar to the the previous section, we believe a simpler characterization may be of importance for fast and crude classification which is not as dependent on the low dimensional phase space structure. Observe the upper diagrams of figure 7 in which the signal $|B(0, t)|$ is presented for three types of reconstructed trajectories. It is clearly seen that the maxima of these signals has quite a different behavior. Now, it follows from Eq. 19 that the expression $|B_0|_{max}$ and $|x_{max}|$, which

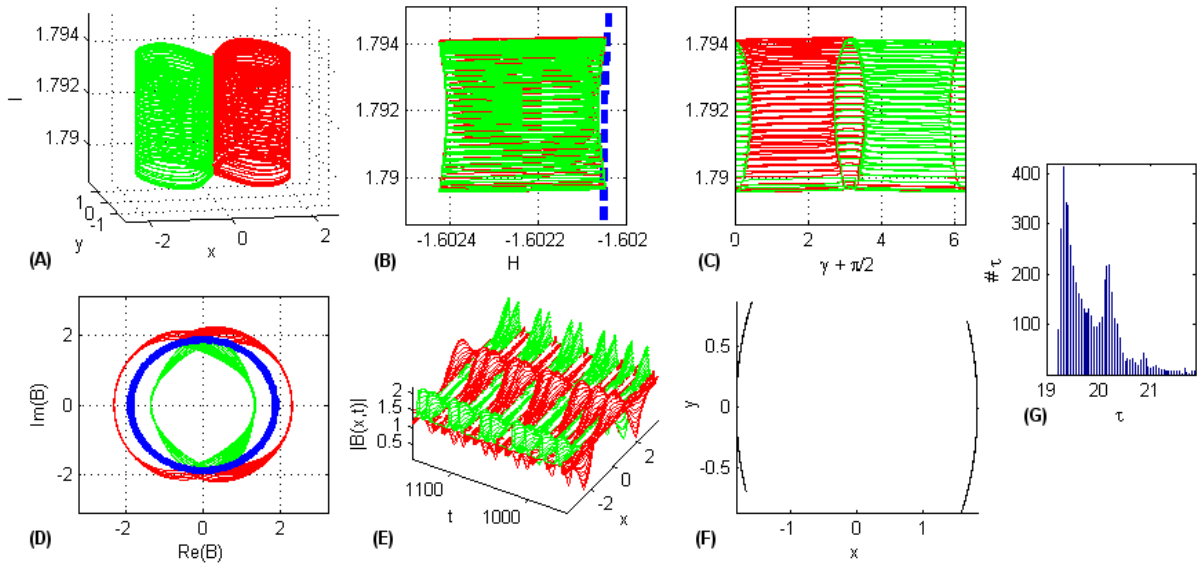

Figure 5. A perturbed orbit near a family of hyperbolic resonant circles for $k = 0.8, \Omega^2 = 1.79, \varepsilon = \frac{1}{\sqrt{2}}10^{-4}$. Initial Conditions: $(c(0), b(0)) = (\sqrt{2}, 10^{-5} + 10^{-5}i)e^{1.8i}$ i.e. $(x(0), y(0), I(0), \gamma(0)) = (10^{-5}, 10^{-5}, 1.79, 1.8)$. An island of stability is detected.

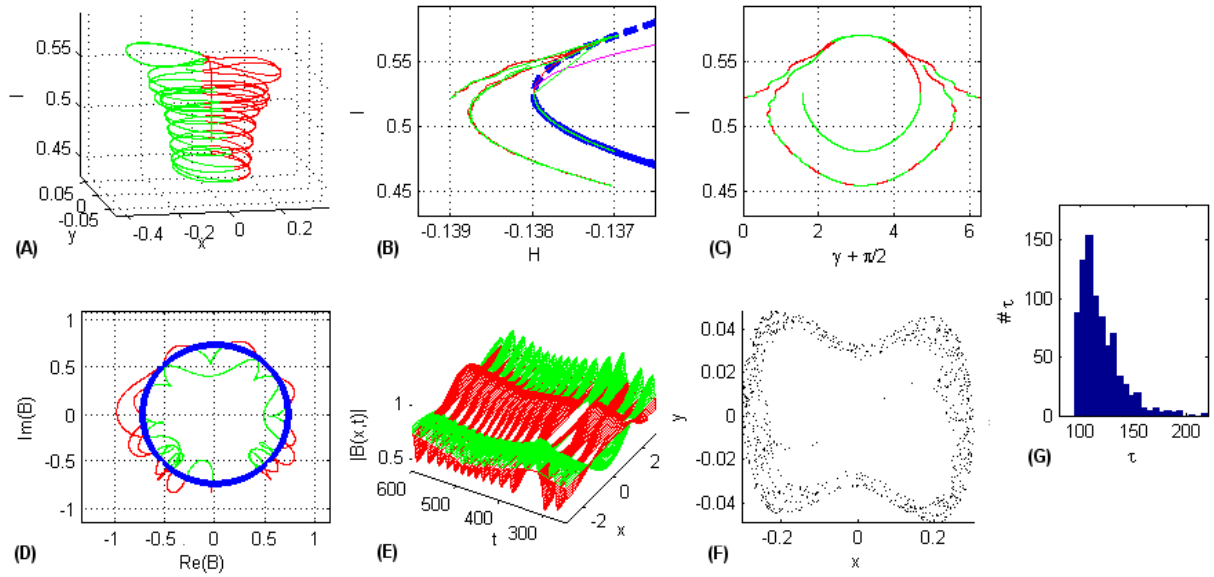

Figure 6. A perturbed orbit near a family of parabolic resonant circles for $k = 1.025, \Omega^2 = k^2/2, \varepsilon = \frac{1}{\sqrt{2}}10^{-4}$. Initial Conditions: $(c(0), b(0)) = (\sqrt{2}, 10^{-6})$ i.e. $(x(0), y(0), I(0), \gamma(0)) = (10^{-6}, 0, 1, 0)$.

is the intersection of the homoclinic orbit to the plane wave with the x-axis, are analogous. Since at homoclinic chaos and at hyperbolic resonance the trajectories follow closely the separatrix, the narrow distribution of the maximal values $|x_{max}|$ (and hence $|B_0|_{max}$) measures the non-uniformity of the cross-section of the chaotic zone with the x-axis near $|x_{max}|$. On the other hand, at parabolic resonance the trajectories pass gradually from the vicinity of elliptic circles to the vicinity of hyperbolic circles and vice versa and this results in a gradual change in x_{max} and correspondingly in $|B_0|_{max}$, see the (x, y, I) diagrams in Figs. 4,5 and 6.

Therefore, we define the set of maximal values of

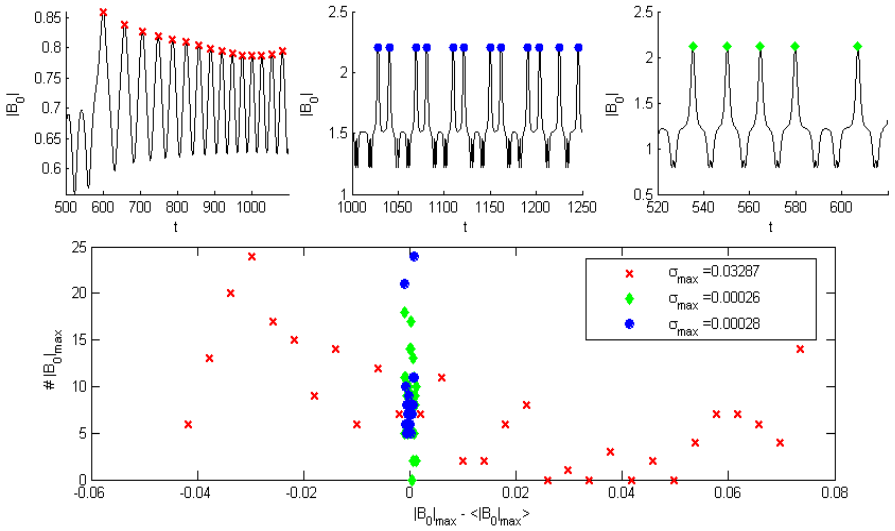

Figure 7. Upper graphs (from left to right): short evolution of $|B(0,t)|$ for parabolic resonance, hyperbolic resonance and homoclinic chaos. Lower graph: PDF of $|B_0|_{max}$ and calculation of σ_{max}. The color and the marker correspond to the color and the marker of the maximal points of each type of motion.

$|B(0,t)|$ as:

$$|B_0^j|_{max} = |B(0,t_j)| \text{ s.t. } \frac{d}{dt}|B(0,t_j)| = 0 \;\&\; \frac{d^2}{dt^2}|B(0,t_j)| < 0 \;\&\; |B(0,t_j)| > B_{pw} = \frac{1}{\sqrt{2}}|c|,$$

where the last inequality guaranties that we consider only the maximal values of x on the right half normal plane in our generalized action-angle presentation. In Fig. 7 we show the PDF of $|B_0|_{max}$ for fixed $\varepsilon = \frac{1}{\sqrt{2}}10^{-4}$, from which we substantiate that there is a different distribution of $|B_0|_{max}$ for different types of motion. To quantify this observation, we compute the normalized standard deviation σ_{max} of the set of maximal values of $|B_0|_{max}$:

$$\sigma_{max} = \frac{\sqrt{< |B_0|_{max} >^2 - < |B_0|^2_{max} >}}{< |B_0|_{max} >}. \quad (20)$$

We assert that σ_{max} supplies a crude measure for the width of the chaotic zone in the x-y plane and hence may be used to distinguish between the trajectories. Indeed, it is clear from figure 7 that for a fixed ε, σ_{max} of a parabolic resonant orbit is much larger from the σ_{max} of a hyperbolic resonant orbit or of a chaotic orbit near a hyperbolic periodic orbit.

In Fig. 8 we examine the dependence of σ_{max} on the perturbation parameter ε. To construct Fig. 8 we integrated, for each case and each ε value, 10 initial conditions all having the same (I,x,y,γ) values as in Figs. 4-6, for a time interval which has a sufficient number

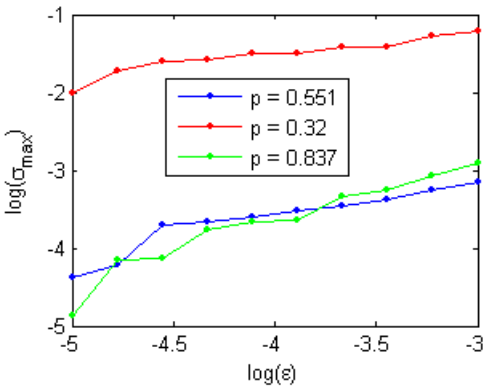

Figure 8. Dependence of σ_{max} on ε.

of $|B_0|_{max}$ samples. Another and more reliable possibility, which we intend to apply in further study, is to choose the same time interval in all three cases. Our assertion, that σ_{max} essentially measures the width of the chaotic zone, implies that σ_{max} should be of order $O(\varepsilon^p)$: for homoclinic chaos we expect $p \simeq 1$, for hyperbolic resonance $p \simeq \frac{1}{2}$ and for parabolic resonance we expect that $0 < p < \frac{1}{2}$. The fitted slopes of Fig.8: $p_{hc} = 0.837 \pm 0.182$, $p_{hr} = 0.551 \pm 0.159$ and $p_{pr} = 0.32 \pm 0.086$ support our assertion. In particular, the slope for the parabolic resonance is well separated from the other cases. In our example, precise distinction between hyperbolic resonance and homoclinic chaos is achieved as well. However, the value of p_{hr} is not as robust as p_{hc} and p_{pr} are. In particular, it appears that our choice of parameters which insure that $\Delta\gamma \simeq \pi$ is essential for obtaining robust results. Other parameter values produce in many cases $p_{hr} \simeq 1$, and indeed in these cases most initial conditions near hyperbolic resonance appear to be indistinguishable from

those starting near hyperbolic periodic orbits.

6 Conclusions

In this paper we characterized different chaotic solutions of the truncated NLS model. We identified these solutions by analyzing the integrable structure using the hierarchy of bifurcations framework. By introducing the additional parameter Ω, the forcing frequency, we demonstrated that we can *control the type of chaotic behavior in the truncated model at a fixed periodic length*. Furthermore, we proposed a simple statistical measure for distinguishing between the variety of chaotic solutions. We have seen that this tool works well in distinguishing between parabolic resonance and the hyperbolic trajectories, but it is not robust in distinction between hyperbolic resonance and homoclinic chaos. Further investigation of this tool and its performance on a variety of perturbed solutions is under current study, as is the design of other simple tools for a precise classification of chaotic orbits near the plane wave solution. One would hope that such methodology will help in the classification and comparison of the perturbed PDE solutions with the truncated model solutions.

Acknowledgements. *This research is supported by the Israel Science Foundation (grant no. 926/04) and by the Minerva foundation.*

References

Bishop, A., D.W. McLaughlin, M.G. Forest and E II Overman (1988). Quasi-periodic route to chaos in a near-integrable pde: Homoclinic crossings. *Phys. Lett. A* **127**, 335–340.

Bishop, A. R. and P. S. Lomdahl (1986). Nonlinear dynamics in driven, damped sine-Gordon systems. *Phys. D* **18**(1-3), 54–66. Solitons and coherent structures (Santa Barbara, Calif., 1985).

Bishop, A. R., K. Fesser, P. S. Lomdahl, W. C. Kerr, M. B. Williams and S. E. Trullinger (1983). Coherent spatial structure versus time chaos in a perturbed sine-Gordon system. *Phys. Rev. Lett.* **50**(15), 1095–1098.

Bishop, A.R., M.G. Forest, D.W. McLaughlin and E.A. Overman II (1986). A quasi-periodic route to chaos in a near-integrable pde. *Physica D* **23**, 293–328.

Bishop, A.R., M.G. Forest, D.W. McLaughlin and E.A. Overman II (1990*a*). A modal representation of chaotic attractors for the driven, damped pendulum chain. *Physics Letters A* **144**(1), 17–25.

Bishop, A.R., R. Flesch, M.G. Forest, D.W. McLaughlin and E.A. Overman II (1990*b*). Correlations between chaos in a perturbed sine-gordon equation and a trunctaed model system. *SIAM J. Math. Anal.* **21**(6), 1511–1536.

Bishop, S.R. and M.J. Clifford (1996). The use of manifold tangencies to predict orbits, bifurcations and estimate escape in driven systems. *CHAOS SOLITONS & FRACTALS* **7**(10), 1537–1553.

Bolotin, S. V. and D. V. Treschev (2000). Remarks on the definition of hyperbolic tori of hamiltonian systems. *Regul. Chaotic Dyn.* **5**(4), 401–412.

Cai, David, David W. McLaughlin and Kenneth T. R. McLaughlin (2002). The nonlinear Schrödinger equation as both a PDE and a dynamical system. In: *Handbook of dynamical systems, Vol. 2*. pp. 599–675. North-Holland. Amsterdam.

Fomenko, A. T., Ed.) (1991). *Topological classification of integrable systems*. Vol. 6 of *Advances in Soviet Mathematics*. American Mathematical Society. Providence, RI. Translated from the Russian.

G.Kovacic (1993). Singular perturbation theory for homoclinic orbits in a class of near-integrable dissipative systems. *J. Dynamics Diff. Eqns. 5* pp. 559–597.

Haller, G[yörgy] (1999). *Chaos Near Resonance*. Applied Mathematical Sciences; 138. Springer-Verlag, NY.

Haller, G[yörgy] and S[tephen] Wiggins (1995*a*). Multi-pulse jumping orbits and homoclinic trees in a modal truncation of the damped-forced nonlinear schrödinger equation. *Physica D* **85**(3), 311–347.

Haller, G[yörgy] and S[tephen] Wiggins (1995*b*). N-pulse homoclinic orbits in perturbations of resonant Hamiltonian systems. *Arch. Rational Mech. Anl.* **130**(1), 25–101. Communicated by P. Holmes.

Kovacic, G. and S. Wiggins (1992). Orbits homoclinic to resonances, with an application to chaos in a model of the forced and damped sine-gordon equation. *Physica D* **57**, 185–225.

Lebovitz, N.R. and A.I. Pesci (1995). Dynamics bifurcation in Hamiltonian systems with one degree of freedom. *SIAM J. Appl. Math.* **55**(4), 1117–1133.

Lerman, L. M. and Ya. L. Umanskiy (1998). *Four-dimensional integrable Hamiltonian systems with simple singular points (topological aspects)*. Vol. 176 of *Translations of Mathematical Monographs*. American Mathematical Society. Providence, RI. Translated from the Russian manuscript by A. Kononenko and A. Semenovich.

Litvak-Hinenzon, Anna and Vered Rom-Kedar (2004). On energy surfaces and the resonance web. *SIAM J. Appl. Dyn. Syst.* **3**(4), 525–573 (electronic).

McLaughlin, David W. and Edward A. Overman, II (1995). Whiskered tori for integrable PDEs: chaotic behavior in near integrable pde's. In: *Surveys in applied mathematics, Vol. 1*. Vol. 1 of *Surveys Appl. Math.*. pp. 83–203. Plenum. New York.

McLaughlin, David W. and Jalal Shatah (1998). Homoclinic orbits for PDE's. In: *Recent advances in partial differential equations, Venice 1996*. Vol. 54 of *Proc. Sympos. Appl. Math.*. pp. 281–299. Amer. Math. Soc.. Providence, RI.

Neishtadt, A. I. (1975). Passage through a separatrix in a resonance problem with a slowly-varying parameter. *Prikl. Mat. Meh.* **39**(4-6), 1331–1334.

Rom-Kedar, Vered (1997). Parabolic resonances and instabilities. *Chaos* **7**(1), 148–158.

Shlizerman, Eli and Vered Rom-Kedar (2004). Energy surfaces and hierarchies of bifurcations - instabilities in the forced truncated nls. in press.

Shlizerman, Eli and Vered Rom-Kedar (2005). Hierarchy of bifurcations in the truncated and forced nonlinear schr[o-umlaut]dinger model. *Chaos: An Interdisciplinary Journal of Nonlinear Science* **15**(1), 013107.